Journal of Materials Processing Technology, Volume 212, Issue 1, January 2012, Pages 188-197

Liquation and post-weld heat treatment cracking in Rene 80 laser repair welds

Matthew T. Rush[1], Paul A. Colegrove[1*], Zhu Zhang[2] and David Broad[2]

[1]Welding Engineering and Laser Processing Research Centre, Building 46, Cranfield University, Mk43 0AL, United Kingdom

[2] Doncasters Group Limited, Millennium Court, Burton-upon-Trent, DE14 2WR, United Kingdom

*Corresponding Author. Email: p.colegrove@cranfield.ac.uk. Phone: +44 1234 754694. Fax: +1234 754717

Abstract

An extensive experimental study on a nickel-based superalloy, Rene 80 using autogenous laser welding has been undertaken to determine the effect of the process parameters and weld bead geometry on cracking in the as-welded and post-weld heat treated conditions. Little cracking was observed in the as-welded condition with low powers and beam diameters around 2.5 mm. Welding speed had little effect on the incidence of cracking in the as-welded condition. Investigation of the aspect ratio (penetration divided by width) indicated that little cracking occurred in the as-welded condition when the aspect ratio was approximately 0.5. The same effect was observed with the post-weld heat treated samples. An analysis of the microstructures indicated that the cracking was caused primarily by liquation in the as-welded condition and was exacerbated by post-weld heat treatment cracking during the subsequent heat treatment. Finally the study resolved some of the contradictory findings in the literature on the effect of process parameters on the incidence of cracking in the as-welded and post-weld heat treated conditions.

Keywords: Liquation cracking, Nickel Superalloy, Laser welding, Strain-age cracking, Post weld heat treatment cracking, Rene 80, repair welding, PWHT cracking.

1 Introduction

Gas turbines are manufactured with a significant number of nickel-based superalloy components. Nickel-based superalloys are selected due to their excellent high temperature creep resistance, corrosion and oxidation resistance. Donachie and Donachie (2002) described how the superior strength of superalloys is achieved through precipitation strengthening with γ' phase ($Ni_3(Al,Ti)$), and carbides which prevent the grain boundaries from sliding and migrating. Henderson et al. (2004) claimed that due to increasing material and manufacturing costs, gas turbine manufacturers are investigating methods of repairing turbine components using fusion welding. Unfortunately, superalloys, like other precipitation-hardened alloys, are susceptible to liquation cracking during welding, and Post-Weld Heat Treatment (PWHT) cracking during the subsequent post-weld heat-treatment (Donachie and Donachie (2002)), which result in the component not meeting the required specification.

Most of the research on liquation cracking has focussed on the superalloy IN 738, although Sidhu et al. (2009), Shahsavari et al. (2007) and Lim et al. (2002) have investigated Rene 80, which is the subject of this article. In a study on the microstructure of over-aged, directionally solidified Rene 80, Sidhu et al. (2009) found that welding caused constitutional liquation of γ' precipitates, M_5B_3 borides, MC carbides, and M_2SC sulfocarbides in the heat affected zone (HAZ). A similar analysis by Shahsavari et al. (2007) on conventionally cast material showed that the phases that constitutionally liquate depend on the prior state of the material. Therefore, MC carbides and γ/γ' eutectic islands liquate in as-cast material, MC carbides and borides in over-aged material and MC carbides in solutionised material. Liquation cracking occurs when the material, that has been weakened by liquation is subject to contraction stresses from the cooling weld region. In addition, the high temperatures from welding can exacerbate the issue of liquation cracking by causing

further precipitation of γ’ precipitates which harden the microstructure, reduce ductility and cause an additional contraction stress in the material – which in turn adds to the contraction stress from the cooling weld.

Lim et al. (2002) and Sidhu et al. (2008) described how PWHT cracking can further exacerbate the cracking caused by liquation or initiate new cracks. The first stage of the PWHT generally involves solutionising. While heating to the solutionising temperature, further precipitation of the γ’ phase occurs (in addition to the precipitation that may occur during welding which exacerbates the liquation mechanism) and causes further hardening, reduced ductility and contraction of the material. When combined with the welding residual stresses, cracking can occur, both through the nucleation of new cracks and the extension of existing cracks caused by liquation.

Another mechanism that can cause cracking in these high temperature materials is solidification cracking which is described in both Dye et al. (2001) and DuPont et al. (2009). The phenomenon occurs along the centreline of the weld pool during the final stages of solidification when a small amount of liquid remains along the solidification grain boundaries and occasionally interdendritic sites. The contraction strains in the solidifying weld pool cannot be accommodated by the small amount of remaining liquid, and result in a centreline crack. The phenomenon is generally exacerbated by impurities such as sulphur and phosphorus; as well as niobium, boron and zirconium which are intentional additions to these alloys. These elements segregate in the liquid due to poor solubility in the solid phase. Weldability maps (for Gas Tungsten Arc Welding) presented in Dye et al. (2001) indicate that the phenomenon is more likely to occur when the power is high and the welding speed is low. As stated in DuPont et al. (2009), weld pools that have a high depth to width ratio have increased susceptibility to this type of cracking.

One final method of cracking that can occur in nickel superalloys is ductility dip cracking which is explained in DuPont et al. (2009). The phenomenon is caused by a significant drop in ductility at temperatures between the solidus (T_s) and approximately half this value ($0.5T_s$). Although there are a number of theories that explain this drop in ductility, many are based on the theory suggested by Rhines and Wray (1961) who stated that it was caused by grain boundary shearing. Given that most precipitation hardened superalloys contain grain boundary carbides and tortuous grain boundaries that prevent sliding, ductility dip cracking is rarely observed. The phenomenon is more prevalent in solid solution strengthened superalloys, and is usually observed in the weld metal.

Wheras most investigations use Gas Tungsten Arc Welding (GTAW) for repair welding, some recent articles by Egbewande et al. (2010), Idowu et al. (2007), Shinozaki et al. (2000) and Zhong et al. (2005) have demonstrated the advantage of laser welding. This process has a low heat input and the ability to control both the power and beam diameter independently. Electron beam welding has similar advantages and has been investigated by Richards et al. (1994).

Most analyses of liquation cracking in superalloys have focussed on the microstructure, with relatively few studies on the effects of the process parameters. However, Egbewande et al. (2010), Shinozaki et al. (2000), Danis et al. (2010) and Richards et al. (1994) have investigated the effect of increasing welding speed at constant power. The results were inconclusive, with Egbewande et al. (2010) showing a slight reduction, Shinozaki et al. (2000) and Richards et al. (1994) showing an increase, and Danis et al. (2010) indicating that it had little effect. In addition, Danis et al. (2010) demonstrated that the effect of power was more significant than that of speed,

with less cracking being observed with lower power. However, this finding was contradicted by Richards et al. (1994), who found that increased power reduced cracking. Shinozaki et al. (2000) stated that when analysing cracking results it is important to consider the effect of the *weld bead profile* which has a significant effect on the amount of cracking. This finding was supported by Richards et al. (1994) and Boucher et al. (1976) who found that greater aspect ratios (defined as penetration divided by the width) increased the amount of cracking.

Hence, the literature is divided over the effect of the process parameters on liquation cracking. Part of the confusion is due to the limited number of processing conditions investigated in these studies. Therefore this paper describes an extensive investigation of the effect of the power, welding speed, beam diameter and weld bead geometry on cracking in Rene 80 in the as-welded and PWHT conditions. For this purpose, partial penetration autogenous welds were studied and statistical techniques similar to those reported in Pinkerton et al. (2008) and Vitanov et al. (2010) were used to identify the parameters that had the greatest effect on cracking. It should be noted that Sidhu et al. (2008) showed that cracking in autogenous welds is more severe than that in wire-added welds due to the harder and less ductile fusion zone in the former. Hence, autogenous welds may be considered the 'worst case'.

2 Experimental procedure

An IPG YLR-8000 high power fibre laser was used for the experimental work. This laser has a wavelength of 1070nm, and a maximum power output of 8 kW. The beam is delivered through an optical fibre to a Precitec YW50 process head with a collimating focal length of 125 mm and a beam focal length of 250 mm. The process head is mounted on a Fanuc M-170iB/45T robot.

The material used in this investigation was Rene 80, a precipitation hardened nickel-based superalloy. The welding trials were split into four sets, with the first set being performed on a different batch of material to the other three. The two batches possessed similar compositions, which are shown in Table 1.

Table 1 Chemical composition of the materials used in the trials (wt%)

	Al	B	C	Co	Cr	Mo	Ti	W	Zr	S	Fe	Si	Ni
Set 1	3.02	0.011	0.15	8.80	14.2	4.1	4.83	3.70	0.02	<0.005	<1.0	<0.1	Bal
Sets 2, 3 & 4	3.05	0.011	0.16	8.96	14.1	3.99	4.87	3.81	0.01	<0.005	<1.0	<0.1	Bal

The material was investment cast into blocks with dimensions of approximately 220 x 70 x 22 mm. After casting, the material was hot isostatically pressed and solutionised. The blocks were then cut to samples of size 70 x 70 x 22 mm. Before welding, the plates were cleaned with a wire brush, and degreased with acetone.

Each of the welds was 70 mm in length, and the parameter combinations used for three of the four sets are shown in Table 2. For the first set, beam diameters of 0.7 and 1.71 mm were used, whereas for sets 2 and 3 used beam diameters of 2.5 and 5 mm were used. Set 3 was performed at low power and welding speeds, which gave similar conditions to those experienced in manual repair welds with arc based processes. In set 4, some select conditions were repeated from the first set, which was used to determine whether the material from the second batch was more or less susceptible to cracking than the first batch. The parameters for this set are shown in Table 3 and are arranged in ascending order of heat input (power divided by welding speed). The beam diameters were achieved by defocusing the beam to produce an energy density that was near Gaussian, and resembled that of a typical repair weld using GTAW. The beam profile was

measured using a Primes GmbH Focus Monitor with Primes Laser Diagnostic Software 2.73. The beam diameter is defined as the diameter that contains 86% of the beam energy. To protect the laser from back reflection, the head was tilted 10° to the plate surface.

Table 2 Summary of the parameters used for the welding trials. The parameter combinations are a matrix of the values provided.

Set	Beam Diameter (mm)	Power (kW)	Welding speed (mm.min^{-1})	Total number of trials
1	0.7	0.4, 0.86, 1.725, 2.6	100, 200, 400, 600, 800, 1000, 2000, 4000	56
	1.71	1.72, 3.44, 6.9	100, 200, 400, 600, 800, 1000, 2000, 4000	
2	2.5	0.5, 1, 2, 4, 8	200, 600, 1000, 2000, 4000	50
	5.0	0.5, 1, 2, 4, 8	200, 600, 1000, 2000, 4000	
3	2.5	0.5, 0.6, 0.8, 1, 1.5	50, 100, 150	30
	5.0	0.5, 0.6, 0.8, 1, 1.5	50, 100, 150	

Table 3 Parameters used for set 4.

Beam diameter (mm)	Power (kW)	Welding speed (mm.min^{-1})	Heat input (kJ.mm^{-1})
0.7	0.86	2000	0.0258
1.71	3.44	2000	0.1032
1.71	1.72	600	0.172
0.7	2.6	600	0.26
0.7	2.6	400	0.39

Beam diameter (mm)	Power (kW)	Welding speed (mm.min^{-1})	Heat input (kJ.mm^{-1})
1.71	3.44	400	0.516
0.7	1.725	100	1.035
1.71	6.9	100	4.14

Upon completion of the trials, each weld was cut in half, with one half being subjected to the standard PWHT for this material. Sections were taken from each weld in the as-welded and PWHT conditions, and polished in two stages: 6 µm diamond suspension followed by 0.05 µm colloidal silica. Kalling's waterless reagent (2g $CuCl_2$, 40ml HCl and 80 ml methanol) was used to etch the samples for up to 10 seconds to show good definition of the grain structure. A single section was taken for all welding conditions except for the samples from set 4 and the corresponding samples from set 1 (for which the same parameters were used as for set 4). In these cases, five sections were taken by measuring the cracks and then machining approximately 1.0 mm before remeasuring. This was repeated four times to give the five sections and the procedure enabled the variability of cracking to be assessed. The samples were analysed using a Nikon Optiphot microscope with Carl Zeiss Axiovision software to measure the lengths of the cracks. Throughout the analysis, the cracking was measured predominantly using the average crack length (ACL) per section, which was chosen over the total crack length (TCL) because it is less dependent on the weld bead size.

Design Expert 7.1 was used to analyse the data and identify the statistically important factors. Two types of model were used on both the as-welded and PWHT data. The first investigated the effect of power, beam diameter, and welding speed, whereas the second investigated the area of the fusion zone and aspect ratio. The fusion zone area was chosen because it was indicative of the

absorbed power per mm, and will be similar to the absorbed heat input. The aspect ratio is defined as the penetration of the weld bead divided by the width. When analysing the data, the Design Expert software used the following transformations of the ACL data:

$$y' = \frac{1}{\sqrt{ACL + 7.5008}} \qquad \text{(1a – as-welded results)}$$

$$y' = \frac{1}{\sqrt{ACL + 26.53}} \qquad \text{(1b – PWHT results)}$$

The functions are plotted in Fig. 1 and their effect was to compress the ACL data when it became large. Hence the statistical models indicated whether cracking was likely to occur or not rather than the extent of the cracking.

Finally an in-depth analysis of three samples was undertaken with a JEOL JSM-7000F Scanning Electron Microscope (SEM) equipped with an Energy Dispersive X-ray (EDX) spectrometer. Semi-quantitative EDX was performed on the cracks observed in each of the samples. Note that it is difficult to accurately determine the amount of carbon when using EDX analysis, due to unavoidable carbon contamination in the SEM vacuum chamber, so the carbon values presented in this document should be treated with caution, i.e. for qualitative comparison. However, the significant differentials of the carbon content detected are sufficient to identify the carbides in the microstructure. Where possible, the matrix has been measured for reference.

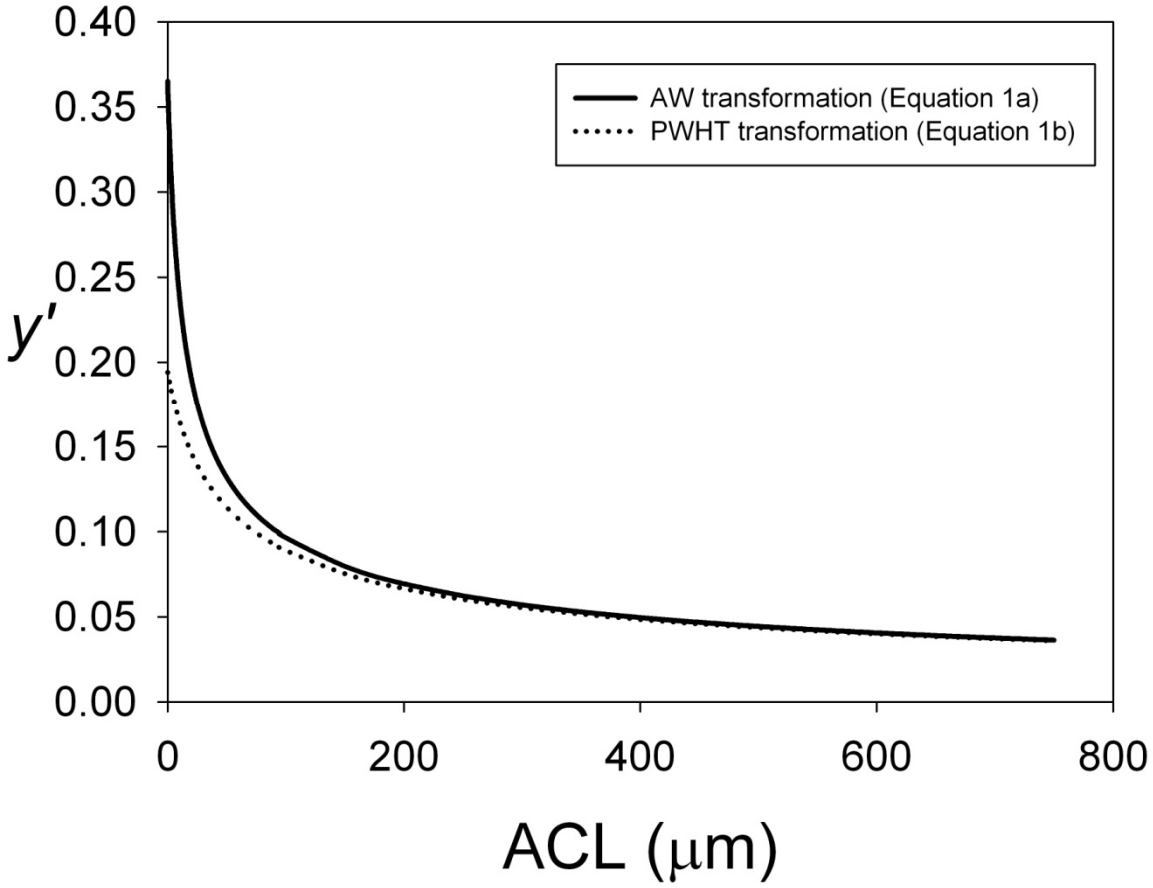

Fig. 1 Plot of the inverse square-root transformations used for the as-welded and PWHT data. The transformation compressed the ACL, making it possible to determine a statistical model to represent the cracking data.

3 Results and Discussion

3.1 As Welded Results

A plot comparing the mean ACLs for the conditions used to check the two batches of material (see Table 2, set 4) is shown in Fig. 2. The mean was obtained from the five sections taken from each sample and the standard deviation is indicated with the error bars. The large standard deviation indicates the significant variability in the ACL. It is also interesting to note that the conditions that caused cracking in one batch of material caused no or minimal cracking in the other.

One of the samples had a very large ACL, which was the consequence of a solidification rather than liquation crack (evidence for liquation cracking will be provided later). This particular sample had a very large aspect ratio of 1.25 which is often associated with this type of cracking phenomenon (DuPont et al. (2009)). Note that no distinction is made between solidification and liquation cracking in the subsequent results and the few occurrences of solidification cracking were always associated with high aspect ratio welds.

On first inspection, it might appear that the first batch was more sensitive to cracking than the second, however a statistical analysis of the results indicated a p-value of 9.95%. As stated in Montgomery (2009) a p-value close to one indicates that the null hypothesis is likely to be true, i.e. the term does not have a significant effect on the output. In statistics a value of less than 5% is usually used to indicate that a factor is statistically significant. Therefore, the chance of the material not being statistically significant is 9.95%, so it is unclear whether there was a difference between the two batches of material. All the subsequent plots show the combined results from all the sets (excluding set 4), and checks were made to ensure that the trends indicated in the global plots were also reflected in the individual plots for particular sets.

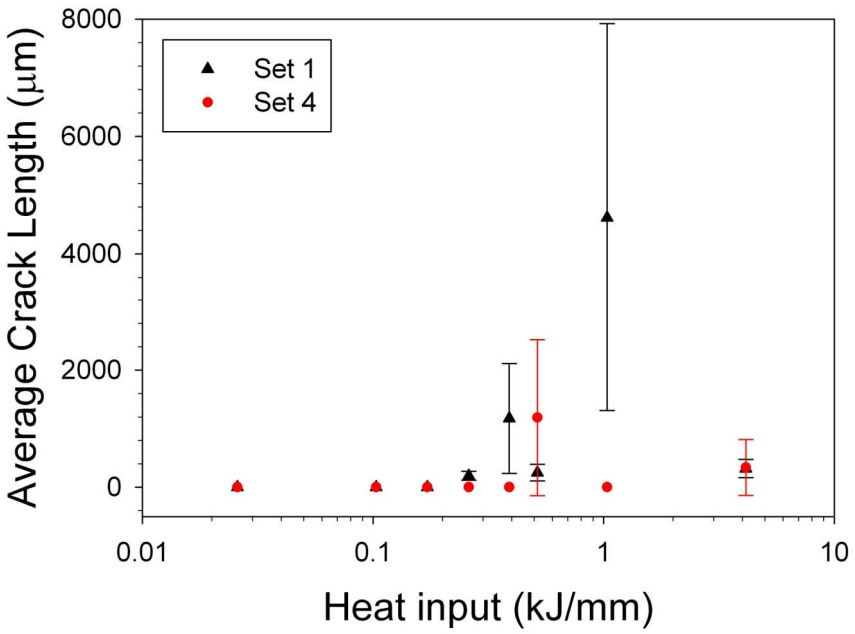

Fig. 2 Plot of the mean ACL vs. heat input for the repeat weld conditions used for the two batches of material. Note that the error bars indicate the standard deviation of the five readings.

Table 4 shows the values of the coefficients of determination (R^2), Adequate Precision, and p-values for the models presented in this paper, which are described in Montgomery (2009). Note that the values of the coefficients of determination were particularly low because of the high variability in the cracking data. i.e. the function was fit between points where cracking occurred ($y' \approx 0.05$) and where it didn't ($y' \approx 0.37$). Hence the distance from the function to these data points was large giving a low value of R^2. Nevertheless the model has been very useful in indicating regions where cracking was minimised. Adequate Precision is a measure of the signal to noise ratio. Given that all the values were above four, this indicated that the model had a reasonable predictive ability. Finally the p-values were all less than 0.01% indicating that the models generated by the software were highly significant.

Table 4 Statistical data for the models presented in this paper.

Statistical Test	As-welded ACL vs. power, beam diameter and welding speed (Fig. 3)	As-welded ACL vs. aspect ratio and Log (fusion zone area) (Fig. 4(b))	PWHT ACL vs. welding speed, power and beam diameter. (Fig. 5)	PWHT ACL vs. aspect ratio and log (fusion zone area) (Fig. 6(b))
Model Type	Reduced Quadratic	Cubic	Reduced two-factorial interactive	Two-factorial interactive
R^2	0.30	0.37	0.53	0.19
Adequate Precision	10.4	11.5	14.4	16.1
p-value	<0.0001	<0.0001	<0.0001	<0.0001

Fig. 3(a) shows a plot of the effects of beam power and welding speed on the likelihood of cracking for a beam diameter of 2.85 mm (from the model). The plot indicates that welding speed had little effect, whereas increasing power increased the likelihood of cracking when the beam diameter was 2.85 mm. Note that when using the transformation shown in Fig. 1, a value of 0.365 corresponds to no cracking and values less than this indicate cracking is likely. Given that welding speed had little effect on the incidence of cracking, a second plot that was independent of the welding speed was created. This is shown in Fig. 3(b) and indicates the combined effect of power and beam diameter. The plot indicates that whereas increasing the power increased the incidence of cracking for beam diameters of 2.5 mm and below, the opposite effect was observed at the largest beam diameter of 5 mm, i.e. cracking actually reduced with increasing power for this diameter. In addition, this plot also suggests that the optimum beam diameter to reduce cracking is around 2.5 mm.

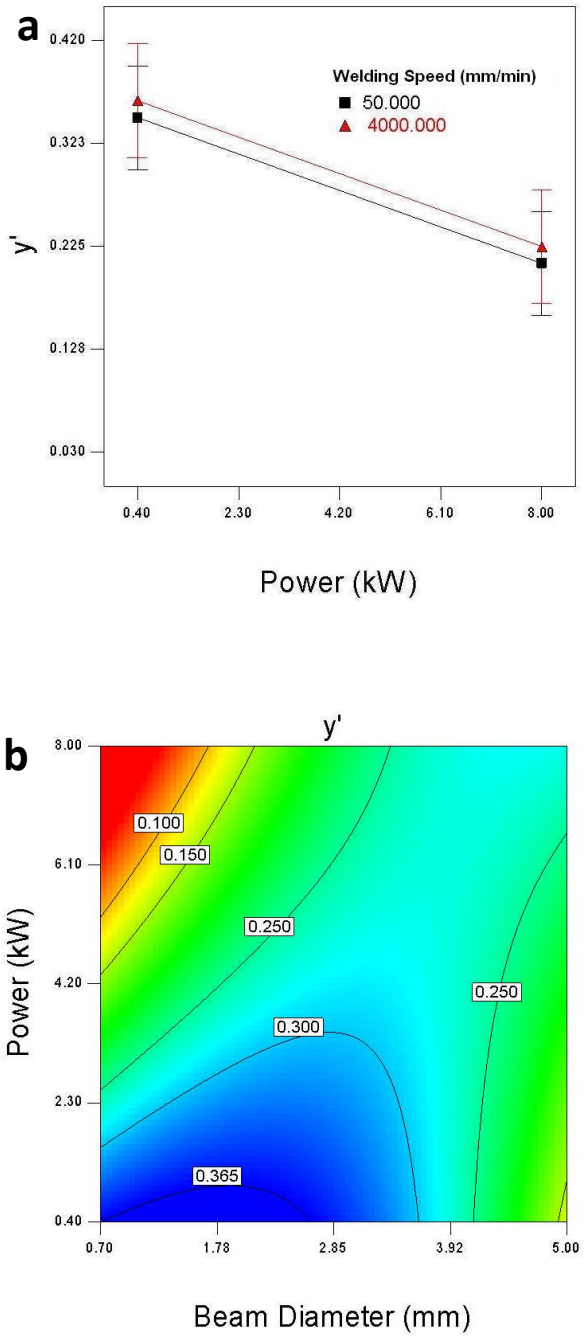

Fig. 3 Effect of (a) power and welding speed (for a beam diameter of 2.85 mm), and (b) beam diameter and power on the transformed ACL, for the as-welded samples. Note that a value of y' = 0.365 corresponds to no cracking.

The empirical equation that was used to generate these results is given by:

$$(\quad + 7.5) \cdot = 0.28 - 0.066 \quad + 0.090 \quad + 0.017 \quad - 0.022 \qquad (2)$$

where

P = power (kW);

d = beam diameter (mm)

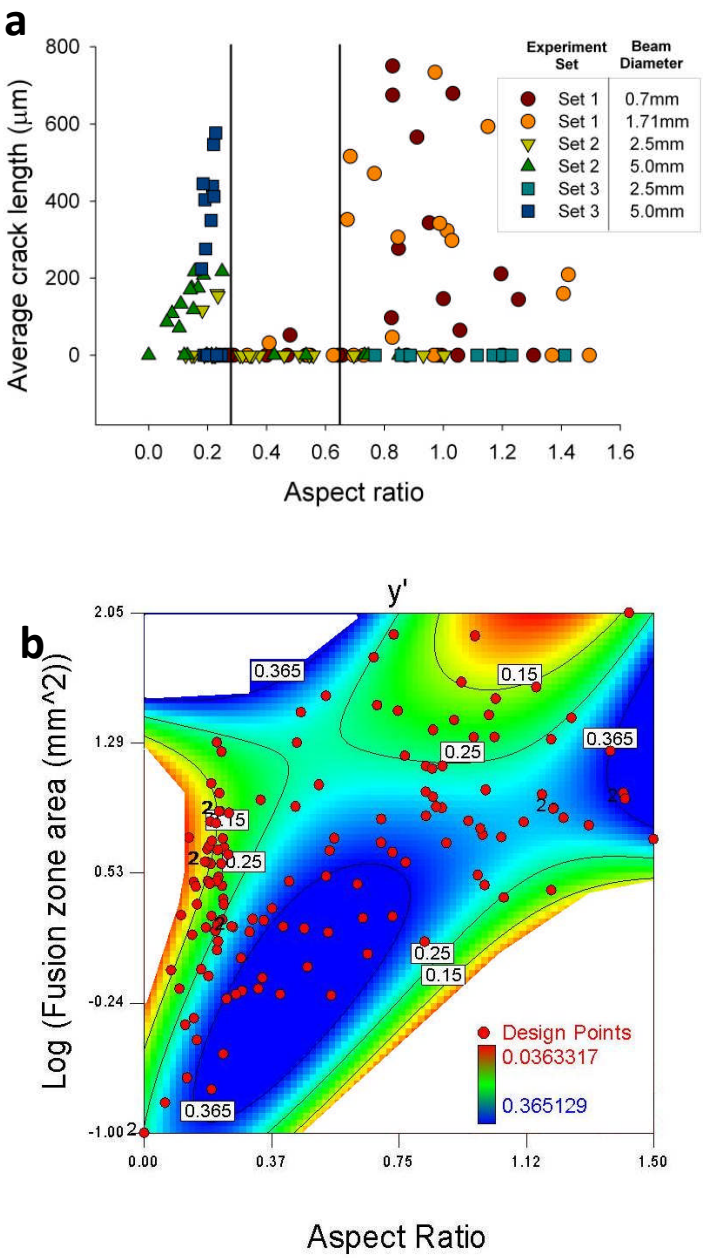

Fig. 4 Plot of the ACL for the as-welded samples vs. (a) aspect ratio and (b) fusion zone area and aspect ratio. Note that a value of y' = 0.365 corresponds to no cracking.

The results in the previous plot suggested that the weld bead shape might be an important factor in predicting the likelihood of cracking. To understand this effect better, the ACL was plotted

against the aspect ratio of the weld bead in Fig. 4(a). Although no cracking was observed (ACL = 0) across the full range of aspect ratios, it was only consistently minimised in the region between 0.25 and 0.65; i.e. the statistical nature of the cracking phenomenon means that consistent reduction in cracking is only observed in this region. In general, the welds with low aspect ratio that showed cracking had the larger beam diameters (2.5 mm and especially 5 mm), whereas the conditions that showed more cracking with the large aspect ratios generally involved the smaller beam diameters.

To understand how the fusion zone area affected the results, the Design Expert software was used to produce a plot of the combined effect of fusion zone area and aspect ratio, shown in Fig. 4(b). Given that the data points are unevenly dispersed across the plot, they are indicated with red dots, and a log scale has been used for the fusion zone area. Note that caution must be used in interpreting this plot, particularly in regions where there are few data points. The plot does however indicate that for very low aspect ratios (i.e. little penetration) cracking was only minimised when the fusion zone area was small. When the fusion area was greater, significant cracking could occur. As the aspect ratio was increased towards 0.5, the range in the fusion zone area where cracking was minimised was enlarged, and the plot indicates that even with large fusion zone areas cracking was low. Cracking increased again when the aspect ratio was increased beyond 0.5. It is likely that the region that showed low cracking at high aspect ratios was a result of the statistical nature of the cracking phenomenon – there are only four data points in this region. Finally, the plot indicates there was a limit in the fusion zone area below which no results were obtained, which increased with the aspect ratio. Hence with the conditions used for the welds it was not possible to obtain any conditions that had both a high aspect ratio and a small fusion zone area. This might be due to the threshold effects associated with the generation of a

keyhole which was needed for the high aspect ratio weld conditions. i.e. a high aspect ratio requires the generation of a keyhole, which was only possible at high power, which in turn generated a large fusion zone area.

3.2 Post-weld Heat Treated Results

Analysis of the PWHT data with the statistical analysis software proved more difficult due to the greater amount of cracking. Therefore, it was only possible to obtain a statistically significant model of the ACL vs. the welding parameters for the first data set. A plot of the transformed ACL vs. power and welding speed for the two beam diameters in set 1 is shown in Fig. 5. A slightly different transformation was used this time, and a value of 0.194 corresponds to no cracking. These plots suggest that welding speed did have an effect on cracking in the PWHT samples, with less cracking occurring as the welding speed increased. In addition, there was slightly lower cracking susceptibility with the smaller beam diameter data which can be seen by comparing the values in the two plots.

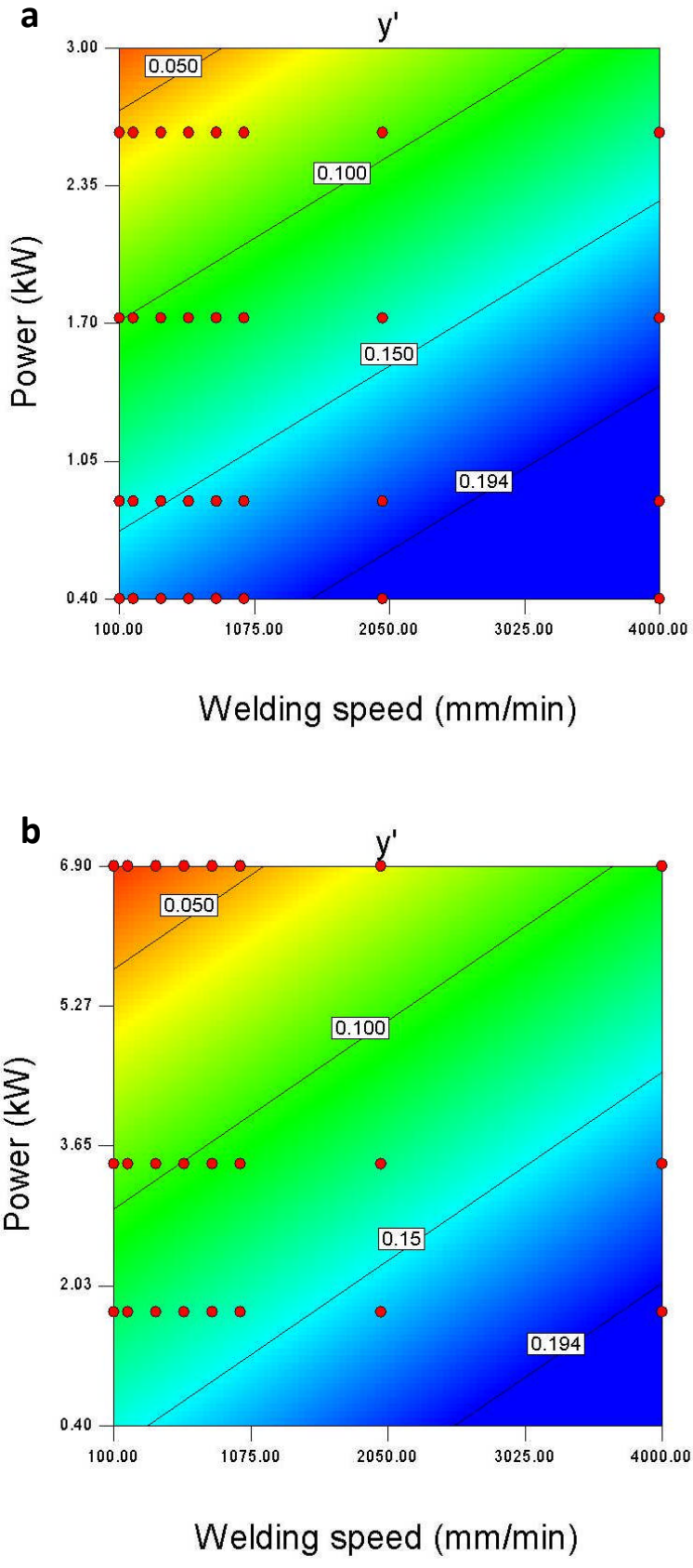

Fig. 5 Plot of the ACL vs. power and welding speed for the PWHT samples from set 1 with beam diameters of (a) 0.7 and (b) 1.7 mm. Note that a value of y' = 0.194 corresponds to no cracking.

The effect of the weld bead shape on the cracking was analysed and is shown in Fig. 6, which includes data from all three sets. Fig. 6(a) shows a plot of the ACL against the aspect ratio, which indicates that cracking was consistently minimised when the aspect ratio was between 0.35 and 0.65. Hence the effect of aspect ratio in the PWHT samples was similar to that in the as-welded samples, except the region over which cracking was minimised was narrower. A statistical model showing the effects of the aspect ratio and fusion zone area for all the data sets is shown in Fig. 6(b). Although this plot indicates that cracking is minimised around intermediate aspect ratios, it also suggests that minimising the fusion zone area is an important factor.

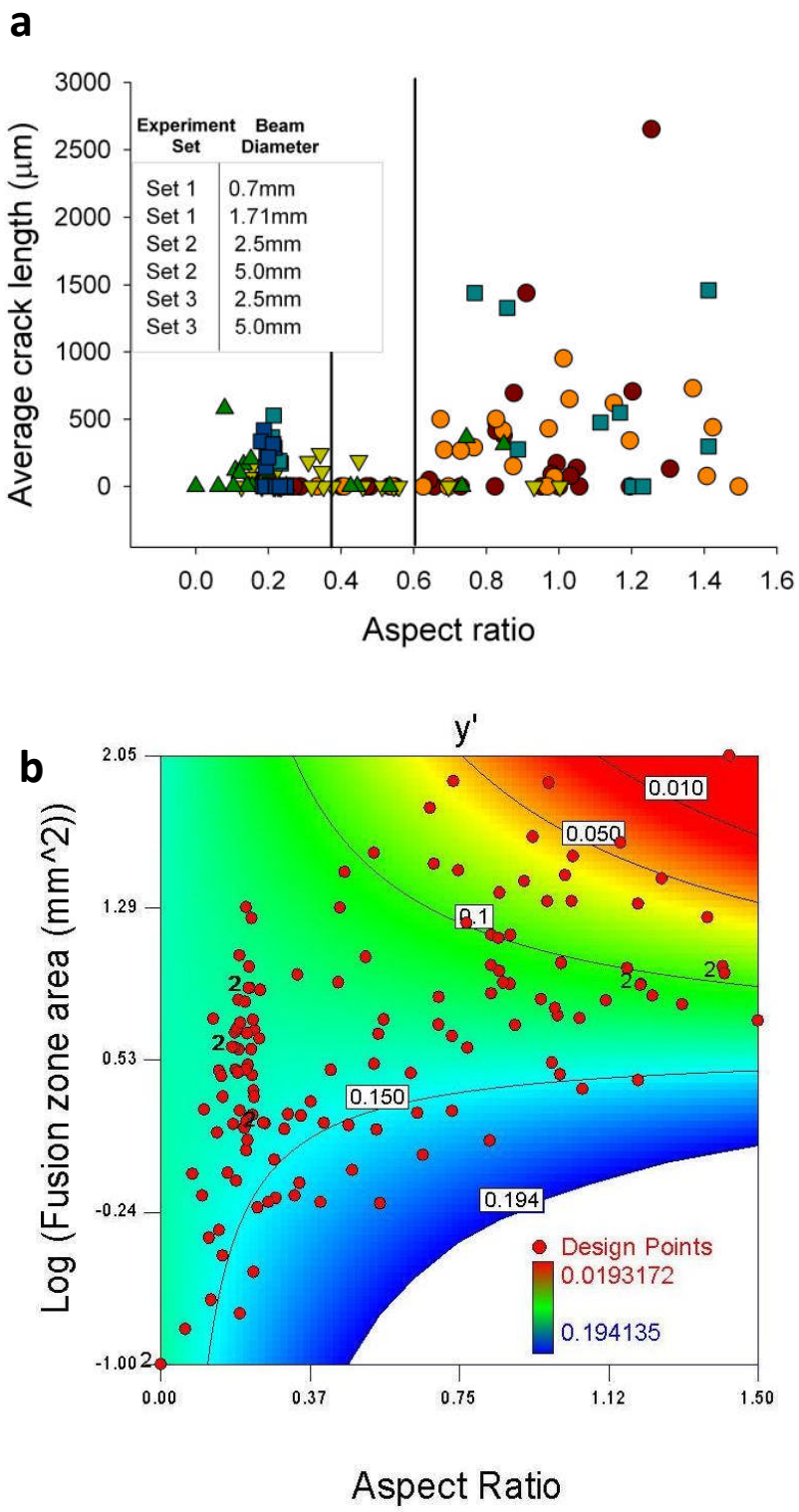

Fig. 6 Plot of the ACL for the PWHT samples vs. (a) aspect ratio and (b) fusion zone area and aspect ratio. Note that a value of y' = 0.194 corresponds to no cracking.

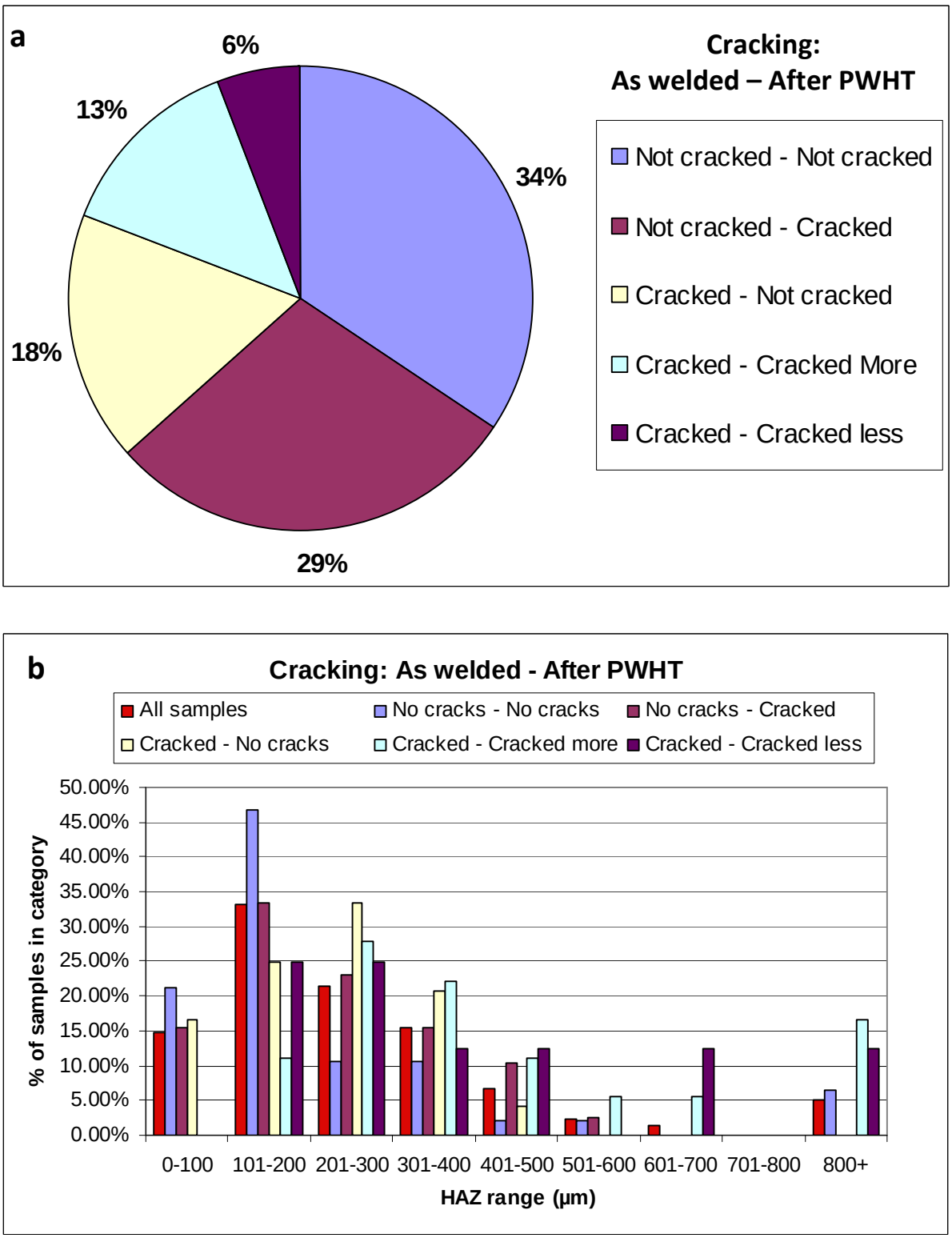

Fig. 7 (a) Pie chart showing the cracking behaviour in all the samples; and (b) HAZ size distribution for the different cracking categories in (a).

The final analysis in Fig. 7(a) compares the cracking before and after PWHT for all data sets. The samples have been split into five categories, which are indicated in Fig. 7(a). In the bottom two categories, cracking occurred in both the as-welded and PWHT conditions and a distinction is made between those that cracked more after PWHT and those that cracked less after PWHT in terms of the total crack length. Across the whole data set, a third of samples showed no cracking in both the as-welded and PWHT conditions (category 1); a third showed no cracking in the as-welded condition, but subsequently cracked during PWHT (category 2); and a third were cracked in the as-welded condition (category 3, 4 and 5). Note that some samples that were cracked initially, subsequently showed no cracking after PWHT, which illustrates the statistical nature of the cracking phenomenon. i.e. the incidence of cracking varied along the length of the sample. The significant variability in cracking along a sample is demonstrated in Fig. 2.

To understand whether the size of the HAZ affected these results, the average HAZ size was measured optically for each sample by averaging its width on either side and underneath the fusion zone. These values were then used to plot a histogram showing the size distribution of the HAZ for the different cracking categories shown in Fig. 7(a), which is shown in Fig. 7(b). The results indicate that for those samples that showed no cracking in either the as-welded or PWHT condition, the HAZ size was relatively small and was centred around 101-200 µm. The samples that did not crack in the as-welded condition but cracked subsequently during PWHT also had a relatively small HAZ zone size that was centred around 101-200 µm; however, in this category, there were relatively more samples with the larger HAZ sizes. For the remaining samples where cracking was observed in the as-welded condition, the HAZ size was shifted towards larger values. Hence the analysis shows the advantage of minimising the HAZ size to reduce cracking in both the as-welded and PWHT conditions.

3.3 Microstructure of the crack

Three macrosections from three samples were selected for further analysis and are shown in Fig. 8(a-c). These samples were selected to cover the full range of aspect ratios. Cracks were observed in all samples. The corresponding SEM images are shown in Fig. 8(d-f) and the results from the EDX analysis are shown in Table 5. Most of the cracks were intergranular and within the HAZ. Random porosity was found in some of the welds, such as the one shown in Fig. 8(b). In samples that had a high aspect ratio and a necked region similar to that shown in Fig. 8(b), the cracks were typically found beside the necked region, under the main weld bead.

The EDX analysis of the low aspect ratio weld in Fig. 8(d) indicated that there was evidence of re-solidified secondary phases (carbides) at the vertical edges of the crack, at the locations marked 1 and 2. It could be argued that the carbides in points 1 and 2 are residual of an original carbide which existed before the weld, but during the weld partial melting of the carbide occurred, allowing some of the liquid to run into and re-solidify on the vertical crack face, visible at point 1. In addition, the wide gap of the crack together with the irregular shape of the crack edge, confirm that this was a liquation crack.

The crack shown in Fig. 8(e) had a wide, irregular and smooth edged morphology with evidence of re-solidified constituents in the crack indicating that the crack formed by liquation. The EDX analysis showed the mixtures were re-solidified γ/γ’ eutectic (points 5-9), and mixture of re-solidified carbide and γ/γ’ eutectic (point 10) together with evidence of residual of an original bulk γ/γ’ matrix (point 12) and residuals of un-melted carbides (points 11, and 13). The final as-welded crack shown in Fig. 8(f) showed further evidence in support of the liquation mechanism, due to the wide sections of the crack morphology, together with the appearance of re-solidified liquid in the

crack. Additionally, the EDX analysis of the re-solidified constituents confirmed that the liquation of secondary phases (carbide and γ/γ' eutectic) were the main cause of the liquation crack.

Finally, one of the PWHT cracks was analysed from a sample which used the same conditions as the as-welded macro in Fig. 8(b). This crack is shown in Fig. 8(g) and two parts are observed: the original liquation crack which had similar morphology to that previously described (although the edges have been affected by the PWHT) at right-upper part of the image; and a much narrower, continuous crack with little evidence of any melting and re-solidification at left-lower part of the image. Further details of the narrow crack are shown in Fig. 8(h), which shows fine crack voids that were formed by stress in front of the tip of the crack. These features indicate the crack was stress induced, formed at relative low temperatures without the liquation reaction, and was therefore likely to be caused by the PWHT cracking mechanism described in the introduction.

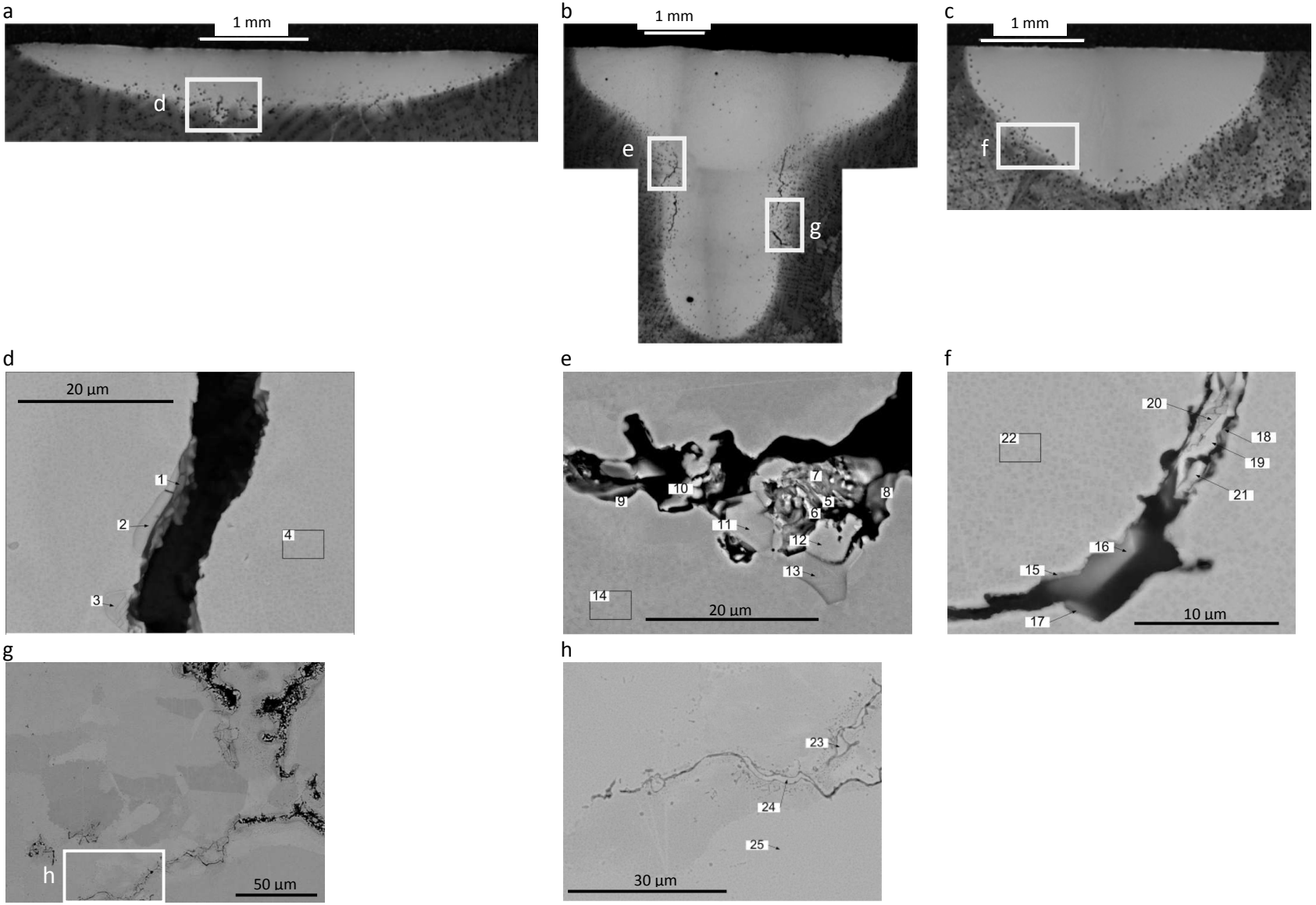

Fig. 8 Macrographs from as-welded samples: (a) low (0.11) aspect ratio (beam diameter = 5 mm, power = 2.5kW and welding speed = 2000 mm.min^{-1}); (b) high (0.83) aspect ratio (beam diameter = 0.7 mm, power = 2.6 kW and welding speed = 400 mm.min $^{-1}$); and (c) optimal (0.55) aspect ratio (beam diameter = 1.71 mm, power = 3.44 kW and welding speed = 2000 mm.min^{-1}). SEM images of liquation cracks observed in as-

welded samples: (d) enlarged image from (a); (e) enlarged image from (b); and (f) enlarged image from (c). (g) An SEM image showing cracking in a similar location in a PWHT sample of the as-welded macro in (b) after heat-treatment; and (h) enlarged image from (g).

Table 5 Results from EDX analysis points shown in Fig. 8. All elements analysed (Normalised). All results in weight%.

No	C	O	Na	Al	Ti	Cr	Co	Ni	Mo	W	Fe	Si	Phase
EDX analysis of Fig. 8(d)													
1	27.43	3.5			34.11	1.85	0.72	5.86	11.05	15.48			M(Ti,Mo,W)C type Carbide
2	27.51	6.65	0.71		36.02	0.89		2.18	16.07	9.98			M(Ti,Mo,W)C type Carbide
3	24.28				43.08	1.41		2.7	17.78	10.75			M(Ti,Mo,W)C type Carbide
4	5.36			2.66	4.56	14.12	9.41	56.74	3.98	3.18			Matrix
EDX analysis of Fig. 8(e)													
5	1.69	0.5		1.04	5.66	13.64	9.87	64.52	1.88	1.2			Mixture re-solidified γ/γ' eutectic
6	3.57	1.23		1.26	5.54	14.17	9.53	63.16		1.54			Mixture re-solidified γ/γ' eutectic
7	6.72	1.02		2.87	4.67	12.85	8.16	56.7	3.51	3	0.51		Mixture re-solidified γ/γ' eutectic
8	4.89	1.09		0.98	4.69	13.52	9.14	63.63	1.45		0.6		Mixture re-solidified γ/γ' eutectic
9	3.83	0.95		0.87	4.65	13.78	8.77	63.56	1.54	1.11	0.61		Mixture re-solidified γ/γ' eutectic
10	10.84	1.84		3.34	6.22	11.59	7.18	51.13	4.2	3.2	0.47		Mixture of carbide and γ/γ' eutectic
11	20.36				45.09	0.85		1.99	9.99	21.72			Residual of M(Ti,W,Mo)C type Carbide
12	3.89			2.9	5.69	14.48	8.94	60.51		3.07	0.53		Residual of a Bulk γ/γ'
13	19.73				46.68	0.91		2.25	13.03	17.41			Residual of M(Ti,W,Mo)C type Carbide
14				3	4.81	15.18	9.43	62.6		4.35	0.62		Matrix
EDX analysis of Fig. 8(f)													
15	28.91	8.79	2.39	2.66	6.66	5.63	3.75	31.2	5.13	3.97		0.9	Predominantly carbide and γ/γ' eutectic
16	29.63	10.11	2.38		29.51	0.88		2.62	9.87	15			M(Ti,Mo,W)C type Carbide
17	19.74	3.61	2.62	0.37	8.22	11.18	6.37	36.54	8.19	2.14	0.58	0.44	Mixture of carbide and γ/γ' eutectic
18	6.66	4.13		4.97	6.08	9.14	6.28	53.85	4.13	3.05		1.71	Mixture of carbide and γ/γ' eutectic
19	6.84	1.2		3.99	4.69	11.66	7.7	56.06	3.97	3.9			Mixture of carbide and γ/γ' eutectic
20	17.94			0.7	30	6	3.11	21.79	7.99	11.97	0.5		Predominantly carbide and γ/γ' eutectic
21	6.9	1.97		3.61	5.98	8.67	6.72	58.69	3.42	3.27		0.76	Mixture of carbide and γ/γ' eutectic
22	5.49			2.45	4.42	13.49	8.05	57.71	4.26	3.51	0.61		Matrix
EDX analysis of Fig. 8(h)													
23	4.62			2.55	10.88	12.40	7.90	53.09	4.20	3.66	0.69		γ'
24	6.06			2.75	7.85	13.00	7.48	54.40	3.68	4.27	0.51		γ'
25	4.59			2.67	3.79	14.04	8.66	58.04	4.17	3.56	0.50		Matrix

4 Discussion

The variability in the cracking can be clearly seen in the large standard deviation in the ACL data in Fig. 2, which made the cracking data difficult to interpret. Ideally many more samples at each condition should have been tested and the *probability* of cracking determined. Nevertheless, the number of samples analysed in this publication is an order of magnitude greater than that reported elsewhere. In addition, it has been possible to determine statistically significant models from the data that was obtained. Throughout the study, it was clear that the microstructure was a significant factor in influencing both forms of cracking. The grain size of the material is large – typically 3.5 mm, hence the degree of segregation and the location of the grain boundary undoubtedly affect both cracking phenomena, and liquation cracking in particular. Hence the location of the grain boundaries relative to the fusion region and HAZ was likely to be one of the main causes of the variability in cracking. This variability could be clearly seen in the different cracking categories shown in Fig. 7(a): in particular where cracking was observed in the as-welded condition, but not after PWHT; and where the TCL after PWHT was smaller than before. The author's believe that this result, which initially appeared suspect, was due to the large variability in the cracking that was observed in Fig. 2 and was potentially caused by the large grain size in the base material.

As noted in the introduction, there is contradictory evidence in the literature regarding the effect of welding speed and power on the incidence of liquation cracking. The current study found little effect of the welding speed, but a more significant effect of

power. It should be noted that although the published literature focussed on the *magnitude* of cracking, this study has focussed on the *incidence* of cracking due to the transformation function applied to the ACL data.

The effect of power depended on the beam diameter, as seen in Fig. 3(b). With small beam diameters, increased power increased cracking, whereas with large beam diameters increased power reduced cracking. This was largely a consequence of the weld bead geometry. As shown in Fig. 4, cracking in the as-welded condition (which was predominantly liquation cracking) was minimised when the aspect ratio was around 0.5. Therefore, when small beam diameters were used with high powers, deeply penetrating welds with large aspect ratios were produced that had a high incidence of cracking. Similarly low powers with the largest beam diameters caused low aspect ratio welds which also had a higher incidence of cracking. In between these two extremes, it was found that a beam diameter of around 2.5 mm (Fig. 3(b)) reduced the incidence of cracking in the as-welded condition. Interestingly, Zhong et al. (2005) reported an optimal beam diameter of 2 mm for laser deposition of IN 738, which is close to the value reported in this study. This beam diameter avoided the extreme aspect ratios that were obtained with either the smaller or larger beam diameters for the range of powers investigated in this study.

The reasons for the significance of the aspect ratio are currently unclear. The aspect ratio may have affected the stresses generated in the HAZ during cooling that caused liquation cracking (in addition to the liquation of grain-boundary phases). In addition,

the high aspect ratio conditions also had a distinct neck around which liquation cracks were often concentrated, as seen in Fig. 8(b). Shinozaki et al. (2000) also observed that liquation cracks were associated with this feature. One explanation is the necked region caused a concentration of stress in an unfavourable orientation, which in turn caused cracking.

Although the PWHT results also indicated a reduction in cracking around an aspect ratio of 0.5, the range of aspect ratios over which it was reduced was smaller than for the as welded condition. The most interesting aspect of these results was the greater importance of the welding speed: increasing the welding speed reduced cracking in the first experimental set. One explanation is that increasing the welding speed typically reduces the size of the HAZ. This may alter the residual stresses within the HAZ and the extent of hardening caused by the precipitation of γ' due to the weld thermal cycle. This is partially supported by Fig. 7(b), which shows how samples that had a small HAZ were less likely to crack after PWHT than those with a large HAZ. An alternative explanation is that the *shape* of the fusion zone changes at the higher welding speeds, giving lower aspect ratio welds, which were less susceptible to cracking for these beam diameters.

Finally the microstructural analysis indicated that while some of the cracks were clearly caused by liquation of carbides, for example those in Fig. 8(d), this was not true in all cases. Both Fig. 8(e & f) indicate substantial quantities of liquation occurred among bulk γ', γ/γ' euteuctic and MC carbides. In an analysis of cracking in a similar nickel

superalloy (IN 738) which was welded in the solutionised state, Ojo and Chaturvedi (2005) found that the γ' particles reacted with the surrounding γ matrix forming a eutectic type reaction which caused liquation of the grain boundaries. This mechanism is consistent with the EDX analysis of the liquated areas in Fig. 8 (e,f).

5 Conclusions

This study on cracking in a nickel-based superalloy has shown that:

1. The welding power significantly affected the incidence of cracking in the as-welded condition, with low powers minimising cracking with a small beam diameter and high powers minimising cracking with a large beam diameter. For the range of powers used in this study, cracking in the as-welded condition was minimised when the beam diameter was around 2.5 mm.
2. Cracking in the as-welded condition appeared to depend on the shape of the weld. In particular, the likelihood reduced when the aspect ratio was between 0.25 and 0.65. A similar result was found with the PWHT samples, although the range of aspect ratios over which cracking was minimised was reduced (0.35 to 0.65). When the fusion zone area was included in the analysis, it was shown that minimising the fusion zone area also helped to reduce the incidence of cracking in the as-welded and PWHT conditions.
3. Increasing the welding speed had little effect on the incidence of cracking in the as-welded condition; however it was found to reduce cracking in the PWHT condition in a subset of the samples.

4. An analysis that correlated the HAZ size to cracking showed that the samples that had no cracking after welding or after PWHT had, on average, a smaller HAZ size than those samples in which cracking occurred.
5. An analysis of the microstructure indicated cracking occurred due to the liquation of secondary phases during welding. These cracks were then observed to extend during the subsequent PWHT via the PWHT cracking mechanism. Solidification cracks occurred in a few of the samples that had a high aspect ratio.

6 Acknowledgements

The authors wish to acknowledge the financial support of Doncasters Group Plc, and the assistance given by Philip Postans in undertaking this work. In addition, the assistance of Flemming Nielsen, Jorn Mehnen, Brian Brooks, David Yapp and Andrew Dyer from Cranfield University was greatly appreciated. The Authors also acknowledge the financial support of the EPSRC through a CASE studentship.

7 References

Boucher, C., Varela, D., Dadian, M. and Granjon, H., 1976. Hot Cracking and Recent Improvement of the Weldability of Nickel Alloys of the Inconel 718 and Waspaloy Types. Revue de Metallurgie.Cahiers D'Informations Techniques. 73, 817-832.

Danis, Y., Arvieu, C., Lacoste, E., Larrouy, T. and Quenisset, J. M., 2010. An investigation on thermal, metallurgical and mechanical states in weld cracking of Inconel 738LC superalloy. Materials and Design. 31, 402-416.

Donachie, M. J. and Donachie, S. J., 2002. Superalloys: a technical guide, 2nd ed ASM International, Materials Park, OH.

DuPont, J. N., Lippold, J. C. and Kiser, S. D., 2009. Welding metallurgy and weldability of nickel-base alloys, John Wiley & Sons, Inc., Hoboken, NJ, USA.

Dye, D., Hunziker, O. and Reed, R. C., 2001. Numerical analysis of the weldability of superalloys. Acta Materialia. 49, 683-697.

Egbewande, A. T., Buckson, R. A. and Ojo, O. A., 2010. Analysis of laser beam weldability of Inconel 738 superalloy. Materials Characterization. 61, 569-574.

Henderson, M. B., Arrell, D., Larsson, R., Heobel, M. and Marchant, G., 2004. Nickel based superalloy welding practices for industrial gas turbine applications. Science and Technology of Welding and Joining. 9, 13-21.

Idowu, O. A., Ojo, O. A. and Chaturvedi, M. C., 2007. Effect of heat input on heat affected zone cracking in laser welded ATI Allvac 718Plus superalloy. Materials Science and Engineering A. 454-455, 389-397.

Lim, L. C., Yi, J. Z., Liu, N. and Ma, Q., 2002. Mechanism of post-weld heat treatment cracking in Rene 80 nickel based superalloy. Materials Science and Technology. 18, 407-412.

Montgomery, D. C., 2009. Design and analysis of experiments, 7th ed John Wiley & Sons, Hoboken.

Ojo, O. A. and Chaturvedi, M. C., 2005. On the role of liquated γ' precipitates in weld heat affected zone microfissuring of a nickel-based superalloy. Materials Science and Engineering A. 403, 77-86.

Pinkerton, A. J., Wang, W. and Li, L., 2008. Component repair using laser direct metal deposition. Proceedings of the Institution of Mechanical Engineers, Part B: Journal of Engineering Manufacture. 222, 827-836.

Rhines, F. N. and Wray, P. J., 1961. Investigation of the intermediate temperature ductility minimum in metals. Transactions of the ASM. 54, 117-128.

Richards, N. L., Nakkalil, R. and Chaturvedi, M. C., 1994. The influence of electron-beam welding parameters on heat-affected-zone microfissuring in INCOLOY 903. Metallurgical and Materials Transactions A. 25, 1733-1745.

Shahsavari, H. A., Kokabi, A. H. and Nategh, S., 2007. Effect of preweld microstructure on HAZ liquation cracking of Rene 80 superalloy. Materials Science and Technology. 23, 547-555.

Shinozaki, K., Kuroki, H., Luo, X., Ariyoshi, H. and Shirai, M., 2000. Comparison of hot cracking susceptibilities of various Ni-base, heat-resistant superalloys by U-type hot cracking test. Study of laser weldability of Ni-base, heat-resistant superalloys (2nd report). Welding Research Abroad. 46, 10-17.

Sidhu, R. K., Ojo, O. A. and Chaturvedi, M. C., 2009. Microstructural response of directionally solidified René 80 superalloy to gas-tungsten arc welding. Metallurgical and Materials Transactions A: Physical Metallurgy and Materials Science. 40, 150-162.

Sidhu, R. K., Richards, N. L. and Chaturvedi, M. C., 2008. Effect of filler alloy composition on post-weld heat treatment cracking in GTA welded cast Inconel 738LC superalloy. Materials Science and Technology. 24, 529-539.

Vitanov, V. I., Javaid, N. and Stephenson, D. J., 2010. Application of response surface methodology for the optimisation of micro friction surfacing process. Surface and Coatings Technology. 204, 3501-3508.

Zhong, M., Sun, H., Liu, W., Zhu, X. and He, J., 2005. Boundary liquation and interface cracking characterization in laser deposition of Inconel 738 on directionally solidified Ni-based superalloy. Scripta Materialia. 53, 159-164.

8 List of Figures

Fig. 3 Effect of (a) power and welding speed (for a beam diameter of 2.85 mm), and (b) beam diameter and power on the transformed ACL, for the as-welded samples.

Fig. 4 Plot of the ACL for the as-welded samples vs. (a) aspect ratio and (b) fusion zone area and aspect ratio.

Fig. 5 Plot of the ACL vs. power and welding speed for the PWHT samples from set 1 with beam diameters of (a) 0.7 and (b) 1.7 mm.

Fig. 6 Plot of the ACL for the PWHT samples vs. (a) aspect ratio and (b) fusion zone area and aspect ratio.

Fig. 7 (a) Pie chart showing the cracking behaviour in all the samples; and (b) HAZ size distribution for the different cracking categories in (a).

Fig. 8 Macrographs from as-welded samples: (a) low (0.11) aspect ratio (beam diameter = 5 mm, power = 2.5kW and welding speed = 2000 mm.min-1); (b) high (0.83) aspect ratio (beam diameter = 0.7 mm, power = 2.6 kW and welding speed = 400 mm.min-1); and (c) optimal (0.55) aspect ratio (beam diameter = 1.71 mm, power = 3.44 kW and welding speed = 2000 mm.min-1). SEM images of liquation cracks observed in as-welded samples: (d) enlarged image from (a); (e) enlarged image from (b); and (f) enlarged image from (c). (g) An SEM image showing cracking in a similar location in a PWHT sample of the as-welded macro in (b) after heat-treatment; and (h) enlarged image from (g).

9 List of Tables